

# Solar Neutrinos—From Puzzle to Paradox

R. S. Raghavan

The solar neutrino puzzle is deepening into a paradox that refutes the basic logic of the reaction chain that powers the sun by the fusion of protons into heavy elements. Experiments now reveal a serious anomaly in the relative neutrino fluxes from the different steps in the chain. Neutrinos from boron-8 at the end of the chain are seen but hardly any are seen from beryllium-7, without which the observed boron-8 cannot be made. The only apparent way to avoid a paradoxical "missing link" in the sun's energy chain is a nonzero neutrino mass, an idea that can be tested in future experiments.

The sun's energy is generated deep in the solar core by the synthesis of He from H by a sequence of thermonuclear fusion reactions. These reactions, referred to as the proton-proton (pp) chain, release nuclear energy by the stepwise production of elements up to B, all of which are transmuted, leaving only He. After millions of years, the released energy reaches the sun's surface and is radiated as sunlight. An exciting possibility arises to look into the center of the sun and directly study the solar energy mechanism in real time, because characteristic neutrinos are emitted during crucial steps in the pp chain. Interacting only through the weak force, neutrinos can escape the sun and reach the Earth in about 8 min. Solar neutrinos have been detected by several experiments, providing a first glimpse of the innermost regions of a star. For the first time, these detections directly reveal the nuclear reactions of the sun's core, and the data are detailed enough to probe solar models. The data also contain surprises that reveal a potential for discovery in an unexpected area, with the sun as the ultimate key for unlocking the elusive secrets of the neutrino itself.

The fusion of  $4\text{H} \rightarrow \text{He}$  by the pp chain is accomplished in three parallel routes, pp-I, -II, and -III (Fig. 1A). The basic step, the  $p+p$  reaction, produces two types of neutrino fluxes  $\phi$ , the strong  $\phi(\text{pp})$  and the weaker  $\phi(\text{pep})$  (where pep stands for proton-electron-proton), marking the pp-I route. These fluxes are determined by basic nuclear physics and the luminosity of the sun, not by solar models. Thus,  $\phi(\text{pp})$  and  $\phi(\text{pep})$  are regarded as standard candle solar neutrino fluxes. All other fluxes depend to various extents on the details of the particular astrophysical model of the sun used, chiefly, the central temperature  $T$ , nominally about 15 million degrees Kelvin. In the pp-II route, the electron capture decay of  ${}^7\text{Be}$  produces the moderately strong neutrino flux  $\phi(\text{Be})$ , varying as  $T^8$ . The weak-

est neutrino flux arises from the decay of  ${}^8\text{B}$  in pp-III, varying as  $T^{18}$ . The CNO reaction chain, the main engine of hot stars, contributes only minor neutrino fluxes in the sun. Quantitative models of the pp chain have been constructed, the most detailed being the standard solar model of Bahcall and Pinsonneault (BP) (1), which are consistent with all observed solar characteristics such as luminosity and radius as well as recent data on helioseismology (2). The testable prediction of the models is the pattern of the solar neutrino spectrum (Fig. 1B), which shows the rarity of the B neutrinos relative to the high pp neutrino rate of  $6 \times 10^{10} \text{ s}^{-1} \text{ cm}^{-2}$  at the Earth.

The first intriguing result on solar neutrinos, as indicated by the pioneering experiment of Davis (3), was that the neutrino flux emitted by radioactive  ${}^8\text{B}$ , the flux most sensitive to details of solar models, is smaller than predicted by theory—the classical solar neutrino puzzle (4). Recently, data from four detectors with different energy windows on the spectrum of Fig. 1B have sharpened the puzzle beyond a deficit in absolute flux compared with model predictions. The new data reveal a severe anomaly in the relative neutrino fluxes from different steps of the pp chain. Neutrinos from radioactive  ${}^8\text{B}$  are observed but, surprisingly, hardly any are observed from radioactive  ${}^7\text{Be}$ , indicating the presence of  ${}^8\text{B}$  but near absence of  ${}^7\text{Be}$  in the sun.

This is a paradox that refutes the logic of the pp chain itself, because the observed  ${}^8\text{B}$  cannot be made without first making  ${}^7\text{Be}$  in the preceding step of the chain (see Fig. 1A). No nuclear or astrophysical remedy for the strange result is in sight. Proposed solutions to the  ${}^8\text{B}$  neutrino-flux deficit only worsen the Be/B anomaly. Effects of a possible nonzero neutrino mass, long seen as one way to explain the B neutrino-flux deficit, now seem the only way to reconcile the Be/B anomaly. The standard model of particle physics prefers only massless neutrinos. Nonstandard neutrino models that relax the zero-mass condition predict as a natural consequence a conversion of the initial electron-type "flavor" of solar neutrinos ( $\bar{\nu}_e$ ) to heavier  $\mu$  or  $\tau$  types that are not detected by the experiments, thus creating a flux loss. Such effects are inherently energy-dependent. They can reduce the low-energy Be electron neutrino flux more than they can the high-energy B electron neutrino flux, thereby neatly explaining the Be/B anomaly and a B electron neutrino deficit.

The emerging Be/B anomaly is crystallizing solar neutrino science into a new phase, with a sharper definition of the problem and a clearer focus on neutrino physics implications. The B neutrino-flux deficit and the Be/B anomaly define the major objectives of future experiments, which are to measure the pivotal Be neutrino flux and to seek explicit neutrino mass effects. For the sizable flavor conversion at  ${}^8\text{B}$  neutrino energies indicated by estimates of the B deficit, future  ${}^8\text{B}$  and  ${}^7\text{Be}$  neutrino detectors may observe mass-specific effects. If, as seems possible, future estimates reduce the B deficit, indicating weaker conversion at high energies, all the neutrino-mass effects expected above become harder to observe. The Be/B anomaly, observed regardless of the B deficit, assures strong conversion at

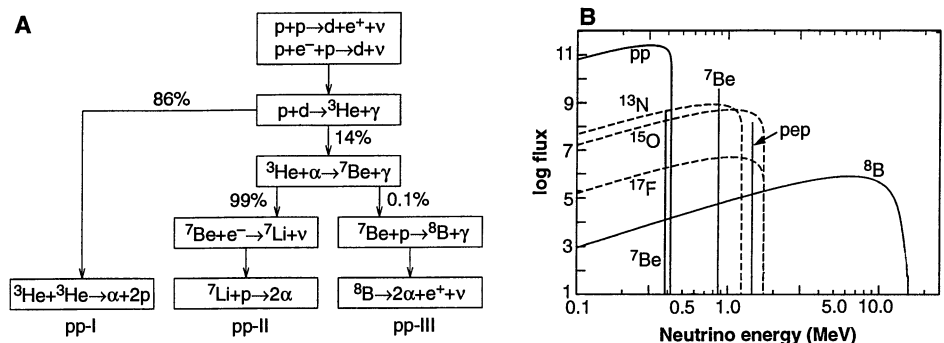


Fig. 1. (A) The p-p reaction chain in the sun. (B) Neutrino spectrum from the sun. [Reproduced from (4) with permission]

The author is with AT&T Bell Laboratories, Murray Hill, NJ 07974, USA.

low energies. I stress that a clear-cut test of general validity for a neutrino mass is a strong deficit in the low-energy standard candle flux of pep neutrinos. The pep neutrino flux is thus the master key to the massive neutrino.

## Neutrino Spectrum from the Sun

*The boron neutrino flux  $\phi(B)$ .* The ideal test of the pp chain is to measure the individual  $\phi(pp)$ ,  $\phi(Be)$ , and  $\phi(B)$ , fixing the branching ratios of pp-I, -II, and -III. So far, the only measured specific neutrino flux is  $\phi(B)$ . The basis of the solar neutrino puzzle is the deficit of the measured  $\phi_{obs}(B)$  compared with the predicted  $\phi_{model}(B)$ . The latter has large uncertainties stemming not only from the solar modeling but, crucially, also from the  ${}^8B + \gamma$  rate of the source reaction  $p + {}^7Be \rightarrow {}^8B\gamma$  controlled by the astrophysical nuclear cross section factor  $S_{17}(0)$  (5). Because  $\phi(B)$  varies directly as  $S_{17}(0)$ , the correct value of  $S_{17}(0)$  has been strongly debated (see Table 1). The low values of  $S_{17}(0)$  in Table 1 (6, 7), for example, would alone reduce  $\phi(B)_{model}$  enough to largely bridge the  ${}^8B$  neutrino-flux deficit. A precision measurement of  $S_{17}(0)$  is technically difficult and subject to questions on the extrapolation of  $S(E)$  from laboratory energies  $E$  ( $\sim 100$  keV) to  $S(0)$  at the very low energies ( $< 1.3$  keV) at the solar core. The BP-adopted value of  $S_{17}(0)$  is based mainly on two experimental results (8, 9) that disagree in their differential cross sections (10). Measurements from the inverse reaction  $\gamma + {}^8B \rightarrow {}^7Be + p$  are in progress. Initial reports suggest (11)  $S_{17}(0) \approx 0.7S_{17}(0)_{BP}$ , thus leaving open a revision to a 30% smaller BP-predicted  ${}^8B$  neutrino flux and cutting the B deficit by more than half.

*The ratio of  $\phi(Be)/\phi(B)$ .* With recent results from several experiments, interest has centered not only on the absolute flux  $\phi(B)$  but also on the ratio of fluxes  $R = \phi(Be)/\phi(B)$ . Measured relative fluxes are, in general, more incisive than an absolute flux compared with a model estimate. The only source of  ${}^8B$  is the reaction  $p + {}^7Be$ , with a

rate  $\sim 10^{-3}$  of the electron capture decay rate of  ${}^7Be$  in the sun (12). Thus, a  ${}^8B$  neutrino signal cannot be observed without the accumulation of a larger solar abundance of  ${}^7Be$  and therefore a large  ${}^7Be$  neutrino signal. The BP model predicts the largest  $\phi(B)$  and thus the smallest value for  $R$

$$\phi(Be)/\phi(B)_{model} = R_{BP} \approx 860 \quad (1)$$

A direct way to decrease  $R$  below the level in Eq. 1 (by 23% at best) is to increase  $\phi(B)$  by using the upper limit on  $S_{17}(0)$  of (8) in Table 1, prospects for which are not bright. The  $\phi(B)$  can be increased astrophysically by enhancing the pp-II branch compared with pp-I through the nuclear S factors; at best, this maintains  $R_{BP}$ . The only idea leading to an  $R$  value less than  $R_{BP}$  [and also  $\phi(B) \rightarrow 0.3\phi_{BP}(B)$ , solving the B-flux deficit (13)] depresses the pp-II branch compared with pp-I by invoking a 10-fold increase in the  ${}^3He + {}^3He$  reaction rate by a hypothetical resonance at very low energies (14). However,  $R$  can be reduced at best only  $\sim 25\%$  below  $R_{BP}$  (13, 15).

In general, ideas to explain the B-flux deficit decrease  $\phi(B)$ ; thus, they only increase  $R$  above  $R_{BP}$ . A smaller  $\phi(B)$  may result directly from a future smaller  $S_{17}$  (by less than a factor 2). In the models, key astrophysical parameters can be varied to nonstandard values, equivalent to lowering the  $T$  of the sun (15). The effect of a lower  $T$ , however, is to reduce  $\phi(B)$  more ( $\propto T^{18}$ ) than  $\phi(Be)$  ( $\propto T^8$ ), increasing  $R$  above  $R_{BP}$ . In summary, despite wide model alterations by nuclear or astrophysical means, the minimum value expected for the Be/B neutrino-flux ratio  $R$  remains very close to  $R_{BP}$ ; for most changes, the revised  $R$  will be larger than  $R_{BP}$ . Thus, if experiments detect an  $R$  markedly lower than  $R_{BP}$ , it is unlikely to be explained by new nuclear data or solar modeling, thus presenting a deep-seated anomaly at odds with the logic of the pp chain.

## Experiments and Results

*Direct detection.* Four experiments are in operation to detect solar neutrinos spectroscopically (Table 2). In Table 2, only

Kamiokande (16) measures a specific solar neutrino flux,  $\phi(B)$ , thus determining pp-III by direct, real-time spectroscopy. Electrons in a water target are scattered by neutrinos and detected via the Cerenkov effect. The energy and track direction of the recoil electron can be measured; thus, the track correlates the event directly to the sun.

*Radiochemical detection.* Three other detectors of a different type provide data on the pp-I and -II branches. On the basis of inverse  $\beta$  decay ( $\nu + A \rightarrow \beta^- + B^*$ ), these detectors operate by irradiating target  $A$  with neutrinos (typically for several weeks) and assaying the separated activity  $B^*$  (17, 18). They are sensitive to all neutrino energies above a threshold  $E_0 = \Delta M$ , the atomic mass difference ( $B^* - A$ ). Unlike Kamiokande, the experimental signal from these detectors mixes neutrino fluxes from several solar sources (Table 2). Therefore, inference of fluxes of individual solar sources needs the model-dependent mixing pattern. Despite drawbacks, these are the only detectors available for observing low-energy neutrinos. The Cl experiment (3) observes primarily  $\phi(B)$  and (to a lesser extent)  $\phi(Be)$ , that is, the pp-III and -II links. The  ${}^{71}Ga$  detectors GALLEX (19) and SAGE (20), with lower thresholds, have a complementary sensitivity pattern focused on pp-I and -II. They are the only devices sensitive to the basic pp neutrinos.

*Results.* Kamiokande has measured the absolute flux  $\phi(B) = 2.9(4) \times 10^6 \text{ cm}^{-2} \text{ s}^{-1}$  and determined that the spectral shape above 7.5 MeV is broadly consistent with the positron decay of  ${}^8B$ . These epochal results are the first to directly measure neutrinos from the sun and demonstrate the operation of the full pp chain by a quantitative measurement of its last link. The results from the Ga detector, which indicate a substantial flux  $\phi(pp)$ , specify the start of the pp chain, completing our first direct glimpse into the solar interior.

Intriguing questions emerge, however, from combining the results in Table 2. The observed fluxes are uniformly lower than predicted, especially the  ${}^8B$  flux derived

**Table 1.** Experimental values of  $S_{17}(0)$ . The reference number is given in parentheses after lead author's name. The unit b, barn, is a unit of nuclear cross section equal to  $10^{-28} \text{ m}^2$  per nucleus.

Lead author	$S_{17}(0)$ (eV b)
Kavanagh (8)	$25.2 \pm 2.4$
Filippone (9)	$20.2 \pm 2.3$
Motobayashi (11)	$16.7 \pm 3.2$
Mukhamedzhanov (analysis) (7)	16.5
Johnson (analysis) (10)	$22.4 \pm 2.1$
Dar (analysis) (6)	15
Bahcall (adopted) (2)	$22.4 \pm 2.1$

**Table 2.** Current solar neutrino experiments and results. 1 SNU =  $10^{-36}$  captures per target atom per second, and  $\phi(B)$  is in units of  $10^6 \text{ cm}^{-2} \text{ s}^{-1}$ . The threshold is given below the experiment name.

Signal	Experiment		
	${}^{37}Cl$ (HOMESTAKE) 0.814 MeV	${}^{71}Ga$ (GALLEX, SAGE) 0.235 MeV	Kamiokande 7.5 MeV (cut)
Observed signal	$2.32 \pm 0.26$ SNU	$78 \pm 10$ SNU	$\phi(B) = 2.9 \pm 0.4$
Predicted signal (BP)	$8 \pm 1$ (100%)	$132 \pm 7$ (100%)	$\phi(B) = 5.7 \pm 0.8$
pp + pep	0.2 (2.5%)	74 (56%)	0
${}^7Be$	1.2 (15%)	36 (27%)	0
${}^8B$	6.2 (78%)	14 (11%)	100%
CNO	0.4 (5%)	8 (6%)	0

from the Cl experiment or Kamiokande (the classical puzzle). The experimental errors and model uncertainties have long fueled a debate on the existence of the  $^8\text{B}$  neutrino-flux deficit and thus of the solar neutrino puzzle (21). The bounds of this debate were set by the observation (22) of the inconsistency between the Kamiokande and Cl results even if one adopts the Kamiokande result as the correct solar  $^8\text{B}$  flux (thus conceding that there is no puzzle). Crucial low-energy experiments with GALLEX and SAGE and extensive analysis (13, 23, 24) unraveled the deeper message: Cl as well as GALLEX and SAGE measurements fail to account for (any)  $^7\text{Be}$  neutrino flux from the sun. Indeed, GALLEX and SAGE results practically account for only the "must see" pp neutrinos despite a sensitivity higher than the Cl experiment to the Be component. Analysis clarifies that the Be/B anomaly is unlikely to be rooted in a "wrong" experiment (25). Thus, the major new result is a serious anomaly in the relative Be/B neutrino fluxes from the sun.

### Be/B Anomaly and Astrophysics

Unlike the B deficit based on a model estimate, the Be/B anomaly is a direct inference from observation. The nonrelevance of solar models can be stressed by using the fluxes  $\phi_i$  from the various neutrino features  $\nu_i$  ( $i = \text{pp, pep, Be, B, or CNO}$ ) constrained only in the aggregate by a quasi-static solar luminosity powered by the pp and CNO reaction chains as (13, 23)

$$2K = \sum_i (Q - 2 \langle E_i \rangle) \phi_i \quad (2)$$

$K$  is the measured solar constant,  $Q$  is the  $4\text{p} \rightarrow \alpha$  fusion energy release, and  $\langle E_i \rangle$  is the average energy carried away by the neu-

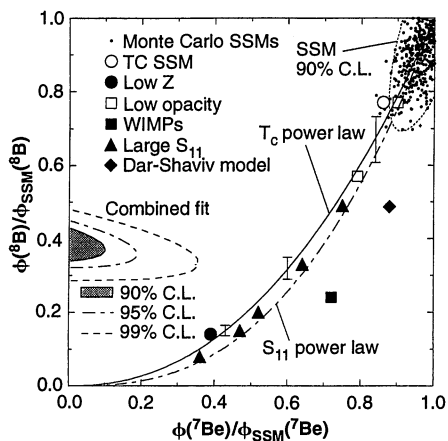


**Fig. 2.** The Be/B anomaly and standard and nonstandard solar models (23). SSM denotes the standard solar model of BP. Dots are results of 1000 Monte Carlo variations of BP. C.L., confidence limit;  $T_c$ , central temperature; WIMPs, weakly interacting massive particles.

trino  $\nu_i$ . The combined results of all the experiments are fit to values of  $\phi(\text{Be})$  and  $\phi(\text{B})$ , allowing fluxes  $\phi_i$  to vary freely; the fit thus accounts for every possible selection of nuclear and solar model parameters and flux predictions (23). The combined fit is shown in Fig. 2 as the shaded area in the  $\phi(\text{Be})$  versus  $\phi(\text{B})$  plane (in units of  $\phi_{\text{BP}}$  for convenience). The best fit gives  $\phi(\text{B})/\phi_{\text{BP}}(\text{B}) = 0.37(4)$  [ $\phi(\text{B}) = 2.2 \times 10^6 \text{ cm}^{-2} \text{ s}^{-1}$ ] and  $\phi(\text{Be})/\phi_{\text{BP}}(\text{Be}) < 0.08$  [ $\phi(\text{Be}) < 3.9 \times 10^8 \text{ cm}^{-2} \text{ s}^{-1}$ ] (23). However, the  $\chi^2$  value of the joint fit is poor, and in fact, excludes it at 96% confidence [ $\chi^2(\text{min})$  occurs for negative values of  $\phi(\text{Be})$ ]. The experimental Be/B anomaly is thus quantified as

$$\phi(\text{Be})/\phi_{\text{expt}}(\text{B}) = R_{\text{expt}} < 180 \quad (3)$$

regardless of the solar model or changes in nuclear data; the sole constraint is Eq. 2 from luminosity. The central question now is, What is the origin of this Be/B anomaly? The incompatibility of an  $R$  value such as in Eq. 3 with the nuclear and astrophysical basis of the sun requiring a much larger  $R$  value such as in Eq. 1 was emphasized earlier. Figure 2 shows this specifically for the  $R_{\text{expt}}$ . Fluxes predicted by the BP model and various nonstandard models advanced to solve the B deficit miss the shaded area without exception. The result of Eq. 3 implies B synthesis without Be, counter to the logic of the pp chain in the sun. Figure 2 stresses that the origins of Eq. 3 are beyond the largely verified nuclear-astrophysical framework of solar energy generation.

### Nonstandard Neutrino Physics

Besides their source reactions, the Be and B neutrinos differ only in their energies, which offer no basis for an astrophysical mechanism for flux loss (26). The only other possible source of the Be/B anomaly is an energy-dependent effect of the neutrino itself, which rules out a standard massless neutrino. Nonzero mass effects, long invoked to solve the much debated B deficit, now become central because the Be/B anomaly is observationally firmer and astrophysically more

paradoxical than a B deficit. A nonzero mass and flavor mixing, the two distinct minimal nonstandard attributes, directly lead to energy-dependent flux changes by neutrino-flavor conversion. Additional assumptions such as neutrino instability or a neutrino magnetic moment can also affect the neutrino flux. I consider only the minimal model which has received the most attention.

**Neutrino flavor conversion.** A solar neutrino is an electron neutrino  $\nu_e$ . If any of the three neutrino flavors  $e, \mu, \text{ or } \tau$  are massive,  $\nu_e$  can be expressed as a mixture of eigenstates of mass ( $m_i, i = 1, 2, \text{ or } 3$ ) and a mixing parameter  $\theta$ . During electron neutrino transport in a vacuum, because of different kinematical phases of the mass states, the mixture evolves into another flavor,  $\mu$  or  $\tau$  neutrino, after a length  $\lambda$ . For the simple case of two flavors,  $\lambda = 4\pi E/\Delta m^2$ , where  $\Delta m^2 = m_1^2 - m_2^2$ . The dependence of  $\lambda$  on  $E$  (neutrino energy) produces an energy-dependent conversion, recorded as a flux loss because the detector registers mostly or only electron neutrinos (27). For large enough mixing,  $\sin^2 2\theta \sim 1$ , the solar electron neutrino flux can be converted almost fully by long-wavelength oscillations (LWOs) (28), if the Earth-sun distance  $R$  precisely matches the oscillation length  $\lambda$ , that is,  $R = (n + 1/2)\lambda$ , where  $n = 0, 1, \dots$ . The electron neutrino survival versus  $E$  for typical LWO models is shown in Fig. 3.

Neutrino transport in matter produces profoundly different phenomena. In the dense solar matter, the kinematical phases are opposed by an interaction phase, depending on the electron density in the traversed matter, because  $e-\nu_e$  scatter has different amplitudes than  $e-\nu_\mu$  or  $e-\nu_\tau$  scatter. At a "resonant" density  $\rho_0 \propto \Delta m^2/E$ , the opposing phases cancel, creating a complete flavor conversion even if  $\sin^2 2\theta \ll 1$  [the Mikheyev-Smirnov-Wolfenstein (MSW) effect (29, 30)]. The MSW effect on  $^8\text{B}$  and  $^7\text{Be}$  neutrino signals is shown in Fig. 4A by isosignal contours in the  $\Delta m^2$  versus  $\sin^2 2\theta$  plane. The MSW resonances occur just above the first horizontal contour at values of  $\Delta m^2 \propto E$ . For  $\Delta m^2 < 0.6 \times 10^{-5} \text{ eV}^2$ ,

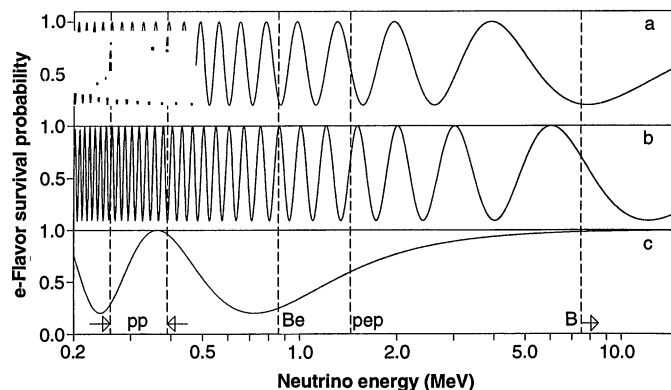


**Fig. 3.** (Curves a and b) Flavor survival versus energy in LWO for BP-based solutions E and B of (32): solution E (in a) and B (in b). (Curve c) Possible solution for a low B-flux deficit with  $\Delta m^2 = 0.6 \times 10^{-11} \text{ eV}^2$ ,  $\sin^2 2\theta = 0.8$ .

$\sin^2 2\theta < 3 \times 10^{-3}$ , the Be flux is mostly converted but not the B flux, thus creating the observed Be/B anomaly.

**Allowed neutrino models.** A comparison of the observed data with model predictions as in Table 2 yields the flux loss versus energy from which allowed parametric ranges in LWO or MSW can be deduced. On the basis of the BP model, joint Monte Carlo fits of all the data have been made (accounting for the correlations in the fluxes, and the theoretical uncertainties) for LWO (31, 32) and for MSW (Fig. 5) (33). The full MSW fit has been repeated with a 30% smaller  $S_{17}(0)$  factor (33); the result is a shift of the small- $\theta_{BP}$  region in Fig. 5A to smaller  $\theta$ , whereas the high- $\theta_{BP}$  region disappears. The effect on the LWO fits is simply to reduce  $\Delta m^2$  by an order of magnitude, which directly reduces conversion at high energies (see Fig. 3, curve c). Because the uniqueness of the BP model is not assured, it is important to explore effects of a nonstandard sun on the fits. These effects can be simulated by a solar core cooler or hotter than in the BP model. A cooler sun implies an initially smaller B flux but a larger Be/B anomaly which must be "fixed" by LWO-MSW, as in the above case of a low  $S_{17}(0)$  leading to a low  $\phi(B)$ . A hotter sun means larger B and Be fluxes and a smaller Be/B anomaly because of the  $T^{18}$  versus  $T^8$  dependence, but it requires a greater degree of neutrino conversion to fit the data. Fits to the data based on the MSW model and with  $T$  allowed to vary freely (32) produce wider bands in Fig. 5B, localized at  $\Delta m^2 \sim 0.5 \times 10^{-5}$  to  $1 \times 10^{-5}$  eV<sup>2</sup>, with  $T = (1 \pm 2\%)T_{BP}$  (32). LWO models have not been fit to a vanishing  ${}^8B$ -flux deficit; a viable possibility with  $\Delta m^2 \sim 0.6 \times 10^{-11}$  eV<sup>2</sup> is shown in Fig. 3, curve c.

The Be/B anomaly summarized by Eq. 3 is obtained under the assumption of standard neutrinos; it stands also if neutrinos convert to undetectable (sterile) species. However, Eq. 3 is affected when strong flavor conversion produces other detectable flavors because the  $\nu$ -e scattering signal in Kamiokande is somewhat sensitive to  $\mu$  or  $\tau$  neutrinos, thus affecting the derived electron neutrino flux result. The smaller the B neutrino-flux deficit, the smaller is the conversion of B neutrinos and the smaller the deviation from the result in Eq. 3. For B neutrino-flux deficits of the BP type or smaller, the Be/B ratio in Eq. 3 is essentially maintained (24). Thus, in this likely range of solar scenarios, the Be/B anomaly is the touchstone of neutrino models. In the MSW scenario, the sharp energy discrimination demanded by Eq. 3 is available only in the low- $\theta$  end of the fit regions in Fig. 5. Analysis fits made in the LWO scenario (32), suggesting very little Be flux loss (see Fig. 3, curve b), are disfavored.

## The Program for Measurement

Future experiments have two major objectives. The first is to measure the specific  ${}^7Be$  neutrino flux on a par with the Kamiokande result on the specific  ${}^8B$  neutrino flux. Astrophysically, data on the specific Be and B fluxes will empirically define pp-II and III (the two model-dependent segments of the pp chain) and thus the sun itself. For neutrino physics, the Be flux value is a key hint for nonstandard neutrinos. The second objective concerns experimental effects explicitly traceable to nonstandard neutrinos. Elegant tests developed for this purpose are based on changes in neutrino fluxes that depend on energy, flavor, or time of year of the neutrino event. None of these properties can change the neutrino flux from an astrophysical standpoint. None of them can change the flux without neutrinos of a nonstandard nature.

**The Be neutrino flux.** Real-time spectroscopy of the  ${}^7Be$  neutrino line at 0.862 MeV demands high signal sensitivity (now limited to energies above 7.5 MeV) and suppression of the ubiquitous radioactivity background at energies below 5 MeV. BOREXINO (34) will address both demands with a detector similar to Kamiokande but which replaces water (its Cerenkov medium) by a liquid scintillator. The larger light yield per MeV (50 times larger than for Kamiokande) helps to detect  $\nu$ -e scattering recoils with an energy as low as 0.1 MeV and to distinguish the "signature edge" of the flat recoil spectrum from the

monoenergetic Be neutrino flux. However, the loss of the vital sensitivity to the neutrino direction makes suppression of the radioactivity background the prime concern. Two characteristics of the BOREXINO (35) experiment provide hope that the background can be adequately suppressed. First, because organic scintillator liquids do not dissolve trace metals, higher purities can be achieved more easily than with a "universal solvent" like water. Second, purity levels attained so far in the liter scale ( $\sim 10^{-15}$  g per gram of scintillator leading to a signal/noise ratio of  $\sim 1$ ) are limited mainly by vessel contamination. Purities are likely to improve considerably in the full-scale BOREXINO experiment because of the smaller surface-to-volume ratio. Nevertheless, because of the key role of the problem, the BOREXINO group has built an underground prototype with a 5-ton scintillator shielded by 1000 tons of water for final live tests now in progress (36). For a 100-ton BOREXINO, Fig. 6 shows the simulated design background and the Be neutrino recoil profile. Compared with the  $\sim 0.25$  per day event rate in present detectors, the Be signal in BOREXINO has an event rate of  $\sim 40$  to 50 per day regardless of the solar model. On the other hand, the measured B flux and the result in Eq. 3 indicate five events per day or less. A larger signal will conflict with results from all the present chemical detectors. Barring this, a BOREXINO signal larger than five events per day can be explained only with an excess signal from neutral current scattering by a non-electron neutrino flux component, thus necessarily indicating nonstandard neutrinos.

**Boron-8 spectral distortion.** Neutrinos from the  $\beta^+$  decay of solar  ${}^8B$  (0 to 14 MeV) have a Fermi-type spectral shape. An energy-dependent flavor conversion (LWO or MSW) will produce a shape distortion

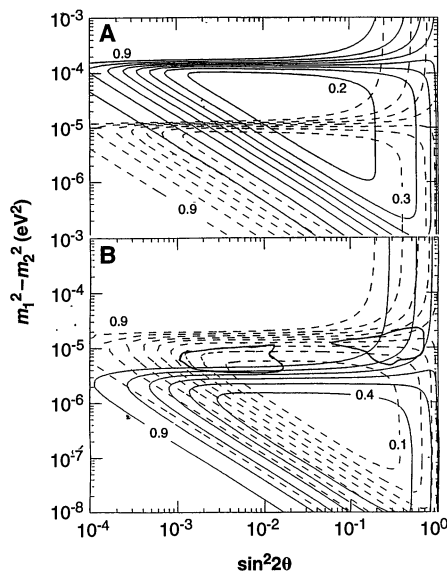


**Fig. 4.** Isosignal MSW contours for (A) the B neutrino signal at Kamiokande (solid line) and the Be neutrino line signal expected in BOREXINO (dashed line) and the (B) pp neutrino signal expected in HERON, HELLAZ (solid line), and the pep neutrino signal in a LiF detector (dashed line). The fit region shown in (B) is from Fig. 5.

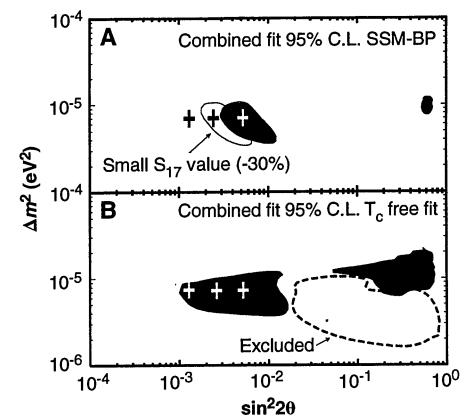


**Fig. 5.** Neutrino regimes allowed by different MSW model scenarios (courtesy of N. Hata). The crosses (left to right) refer to the spectral shapes (b to d) in Fig. 7.

observable in two impending detectors. SUPERKAMIOKANDE (SK) (37) is a 22-kton version of the Kamiokande (0.6 kton)  $\text{H}_2\text{O}$  Cerenkov detector. The Sudbury Neutrino Observatory (SNO) is a 1-kton  $\text{D}_2\text{O}$  Cerenkov detector based on the inverse  $\beta$  reaction:  $\nu_e + d \rightarrow 2p + e^-$  (38). Unlike the  $\nu$ -e scattering signal at SK, the inverse  $\beta$  at SNO yields an electron spectrum linearly related to the electron neutrino spectrum and is thus more sensitive to the neutrino spectral shape. The  $^8\text{B}$  event rates are high,  $\sim 8$  per day (SNO) to 22 per day (SK) at  $E > 5$  MeV. Theoretical spectral deviations of the signal in SNO due to the MSW effect are shown in Fig. 7. In the high- $\theta$  regime of Fig. 5, the shape is undistorted; therefore, the spectral test applies only to the low- $\theta$  areas. In the BP-allowed area (Fig. 5A), the distortion observable in the SNO energy window is significant (curve d). For smaller  $\theta$ , the main conversion shifts to energies below the windows in SNO and SK. Thus, for the regime of a low  $S_{17}(0)$  in Fig. 5A, the observable distortion is small (curve c). The trends are similar for LWO as seen at the B window in Fig. 3 (curves a and b) for the BP regimes and Fig. 3 (curve c) for a low B deficit. Thus,  $^8\text{B}$  spectral effects due to a nonzero neutrino mass may be observable

for low- $\theta$  regimes allowed by BP-size B-flux deficits. The effects will be smaller if the B-flux deficit becomes smaller.

The electron neutrino flux versus neutrino flux of all flavors. Spectral shape effects depend on the conversion of the electron neutrino into another flavor. If the total flux of  $\nu_X$  ( $X = e, \mu, \tau$ ) can also be detected, the ratio of the  $\nu_e$  and  $\nu_X$  signals would be a test of conversion in general (if the new flavor is not sterile, that is, nonreactive). This device is possible in SNO by means of a second reaction,  $\nu_X + d \rightarrow p + n$ , based on neutral weak currents (NCs) (39). The NC signal measures the total solar flux regardless of flavor, to be compared with the charged current (CC) electron signal from the inverse  $\beta$ , which measures only the electron neutrino flux. The flux ratio derived from the NC/CC channels,  $\phi(\nu_X)/\phi(\nu_e) \neq 1$ , verifies flavor conversion. An analysis of the practical sensitivities for NC/CC indicates reliable results for a BP-size B-flux deficit but points to a less unambiguous prospect if the BP B flux is reduced even by  $\sim 20\%$  (40). Weaker conversion at B neutrino energies means less disparity between the NC- and CC-derived B fluxes.

Time variations of the Be neutrino flux. If

the LWO model is the cause of the B-flux deficit, mass-specific effects occur also for the Be neutrino signal. The reason, as seen in Fig. 3 (curves a and b) for a BP-size B-flux deficit, is that the electron neutrino survival oscillates sharply with energy at low energies. Because the  $^7\text{Be}$  flux is monoenergetic, its electron neutrino survival is fine-tuned to a precise match of its conversion length  $\lambda(E)$  to the Earth-sun length ( $R$ ). Even a change in  $R$  of less than 3.5% in the Earth's eccentric orbit detunes the  $\lambda(E) \leftrightarrow R$  match and changes the electron neutrino flux. Thus, the Be signal will vary dramatically with the season, directly demonstrating neutrino oscillations (41). Because predicted variations are strong, BOREXINO may be able to detect this effect. Curve c in Fig. 3 also shows that, for a smaller B deficit [due to, for example, a low  $S_{17}(0)$ ], the low-energy electron neutrino survival varies far more gradually, thus becoming insensitive to small changes in  $R$ . Thus, although the Be flux itself is largely converted as above, seasonal variations of the signal will be small.

### Master Key to the Massive Neutrino

The two clues from the sun for a nonstandard neutrino are the B-flux deficit and the Be/B anomaly. For BP estimates of the B-flux deficit, neutrino-mass effects can be detected by one or another of the above tests. However, if the B deficit is reduced explicitly by future model estimates or is already small implicitly as in substantial parts of the currently allowed neutrino regimes of Fig. 5, the implied  $^8\text{B}$  neutrino conversion is weaker and thus also the sole basis for all of the above neutrino-mass effects. How then to detect a nonstandard neutrino if the only clue is the Be/B anomaly?

The experimental focus in this case is on low energies because, regardless of the B deficit, the Be/B anomaly assures strong conversion at low energies. A decisive low-energy neutrino-mass test is the observation of a deficit in a standard candle flux that is invariant with solar models. The pp reaction and its variant pep reaction are two such standard candles, both emitting low-energy neutrinos. The best mass test should also be general, being applicable with few caveats and regardless of scenario or parameter range. Raghavan *et al.* first pointed out that it is the pep flux that provides such a key (42) rather than the pp flux, the conventional choice, which is barely affected in most current neutrino scenarios.

Consider the MSW effect. Figure 4B shows the isosignal contours for possible experiments such as HERON (43) and HELLAZ (44) designed to detect pp neutrinos and for a LiF detector (42) proposed

**Fig. 6.** Design spectra of BP-predicted signal and background (Bgd.) simulated for BOREXINO (35). Int., internal sources in the scintillator; Ext., external sources.

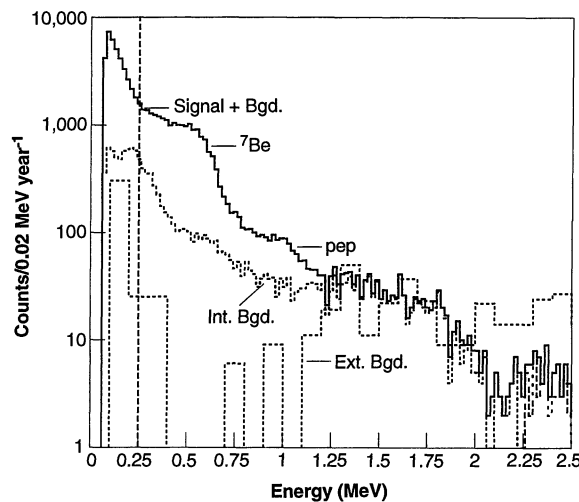
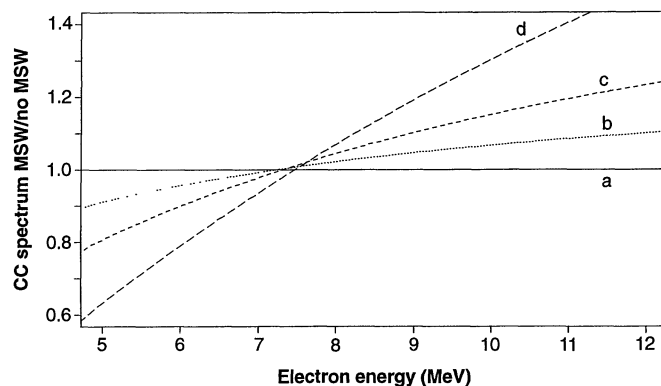


**Fig. 7.** Theoretical CC spectral deviations in SNO for MSW/no MSW (for equal signals  $> 5$  MeV): curve a, high- $\theta$ ; and curves b to d, low- $\theta$  as marked in Fig. 5. In practice, the deviations will be  $\sim 60\%$  of those above. Most of the signal occurs at  $< 10$  MeV.



for the pep neutrino line. Because the two energies differ by a factor of  $\sim 4$ , the MSW resonance sets in at different  $\Delta m^2$  values. The allowed band from Fig. 5B lies in between, showing that the pp flux is always nearly intact, whereas the pep flux is reduced by at least a factor of 2, and typically a factor of 5. Similarly, in Fig. 5, A and C, for LWO scenarios consistent with the Be/B anomaly (with large or small B deficits), the pep flux is  $\sim 50\%$  converted.

On the theoretical side, the pep deficit test applies, whether neutrinos convert to fertile or sterile flavors. With few caveats—a clear-cut verdict and a general validity, especially in wide regimes where all other mass tests may fail—a deficit in the pep neutrino flux is the master key to a massive neutrino. The impact of a pep deficit would be enhanced if the pp neutrino flux is shown nearly intact as well. The different effects on two standard neutrino fluxes bracketing the Be neutrino line would highlight the characteristic energy dependence of the electron neutrino-flux loss.

### The Quest for pep Neutrinos

**BOREXINO.** Assuming that 5-ton tests are successful, the earliest source of data on the pep flux may be BOREXINO. The simulation in Fig. 6 shows the pep  $\nu$ -e scattering plateau at 0.8 to 1.1 MeV, with a solar model-independent electron neutrino event rate of  $\sim 900$ /year in the window. The design signal/noise ratio of 1 to 2 is less favorable than for the Be line. However, the background profile beyond the plateau is nearly flat, enabling reasonable extrapolations into the pep window. Thus, a background at the design level of Fig. 6 can permit at least firm upper limits to be set that rule out an undepleted pep flux. A result that establishes strong depletion of the Be and pep fluxes will verify the Be/B anomaly and a massive neutrino. The prime physics and design objectives of BOREXINO should now include spectroscopy of the pep neutrino line. Further, Fig. 6 also shows the sharp signal rise due to the pp neutrino flux at energies below 250 keV. The observability of the pp signal depends on the near total absence of  $^{14}\text{C}$  in the scintillator, a possibility that is not ruled out because the liquid is petroleum-derived. The question will be clarified in the ongoing 5-ton tests.

**HELLAZ.** The pep flux, though small, is monoenergetic. A sharper energy resolution than in Fig. 6 (therefore a higher signal/noise ratio) can lead to quantitative measurements of this line flux even with weaker signal rates. Two proposals of high-resolution line spectroscopy are relevant for the pep neutrino flux: HELLAZ and the LiF cryogenic detector. HELLAZ (44) is based on  $\nu$ -e scattering in a 20-ton

target of high-pressure He. The recoil electron track can be imaged by time projection chamber techniques and its energy and direction measured. It is claimed that despite severe multiple scattering at these energies it is still possible at these pressures to deduce the track direction. Assuming that the observed events are due to the scattering of a monoenergetic neutrino of known energy coming from the direction of the sun, the original line itself (instead of the normal plateau as in Fig. 6) can be reconstructed because the scattering angle and the recoil energy are fixed event by event. This elegant idea and the design of HELLAZ are aimed at the high-flux pp neutrinos and the Be neutrino line. The design is clearly extendable to the low-flux pep line.

**LiF cryogenic detector.** A different approach to line spectroscopy of nuclear events is by means of thermal or acoustic signals in crystals at cryogenic temperatures ( $\ll 1$  K) (45). Kiloelectron volt-class energy resolution has been demonstrated in crystals such as LiF (46). As a direct-counting solar neutrino detector, a LiF cryogenic device can yield unique information independently on astrophysical and neutrino physics aspects because the  $^7\text{Li}$  (92.5% of Li) target offers, like in SNO, two neutrino reactions based on NC and CC, but in this case, for the crucial low-energy solar neutrinos (42). The CC mode,  $\nu_e + ^7\text{Li} \rightarrow e^- + ^7\text{Be}$ , produces a line signal at 0.58 MeV from the pep line, which can directly reveal flavor conversion. The NC mode,  $\nu_x +$

$^7\text{Li} \rightarrow \nu_x' + ^7\text{Li} + \gamma$ , produces a gamma ray line at 0.478 MeV which measures the integrated flux  $\phi(\nu_x)$  [pep +  $^7\text{Be}$  +  $^8\text{B}$  + (CNO)] of the same solar sources as the Cl chemical detector (although it emphasizes Be over B). The important difference is that whereas Cl measures only the electron neutrino flux subject to conversion, the Li NC signal measures that flux regardless of conversion. In contrast to the Cl result, the Li NC signal can at last find the missing Be flux and explicitly resolve the paradox. The independent roles of the CC neutrino probe and the NC solar probe are illustrated in Fig. 8 by the Li "fingerprints." Note, in particular, the clear discrimination of an astrophysical origin of the flux deficits in the current results (Fig. 8B) and well-defined solutions based on massive neutrinos (Fig. 8, D to F). Initial studies of a LiF cryogenic solar neutrino detector (42) suggest that, with a feasible 1 to 2 keV energy resolution (1/50 that in Fig. 6), a 4-ton device can establish a pep-flux deficit in a live time of  $\sim 1$  year.

### Concluding Remarks

Solar neutrino science is entering a new phase. The central thrust now comes from a measured anomaly of relative neutrino fluxes that poses a basic paradox if neutrinos are massless. The history of weak interactions is punctuated by long episodes of persistent puzzles which, when ultimately solved, led to landmark discoveries. For example, the puzzle of the continuous beta spectrum led to the discovery of the neutrino itself, and the solution to the  $\tau$ - $\theta$  puzzle revealed parity violation and the left-handed neutrino. In both cases, the puzzles gradually crystallized into paradoxes that questioned the very logic of current knowledge, setting the stage for revolutionary solutions. The solar neutrino story seems to have reached this stage with the Be/B anomaly. Are we now witnessing the overture to another heroic episode, this time leading to the discovery of the massive neutrino?

### REFERENCES AND NOTES

1. J. N. Bahcall and M. Pinsonneault, *Rev. Mod. Phys.* **64**, 885 (1992); see also Proceedings of the *Solar Modeling Workshop*, Seattle, WA, 24 March 1994 (Institute of Nuclear Theory, Seattle, WA, in press), for updated reviews.
2. D. R. Gough, *Philos. Trans. R. Soc. London A* **346**, 37 (1994).
3. R. Davis Jr., in *Frontiers of Neutrino Astrophysics*, Y. Suzuki and K. Nakamura, Eds. (Tokyo University Academy Press, Tokyo, 1993), p. 47.
4. J. N. Bahcall, *Neutrino Astrophysics* (Cambridge Univ. Press, Cambridge, 1989).
5. The reaction rate of two nuclei of mass numbers  $A_1$ ,  $A_2$  and atomic numbers  $Z_1$ ,  $Z_2$ , moving with relative speed  $v$  and energy  $E$ , is given by the energy-dependent cross section [see (4)]:  $\sigma(E) = [S_{A_1 A_2}(E)/E] \exp(-2\pi Z_1 Z_2 e^2/\hbar v)$ . The value of  $S(E)$  is extracted from measured values of  $\sigma(E)$  using models of nuclear reactions.

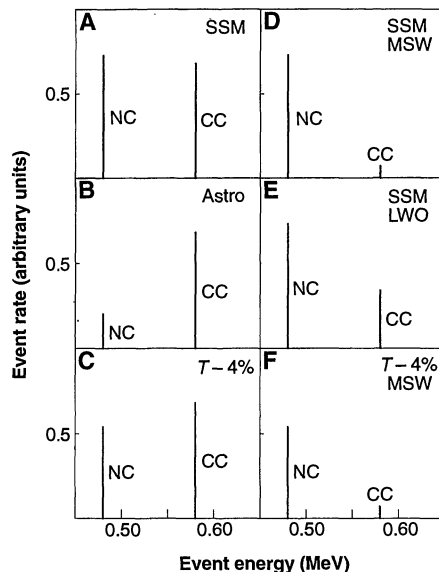


**Fig. 8.** (A to F) NC and CC line-spectra in LiF detector for neutrino and solar scenarios. SSM denotes predictions based on the standard solar model of BP. Astro assumes all current flux deficits are astrophysical because of smaller original model-dependent fluxes.  $T-4\%$  indicates a 4% lower central temperature of the sun.

6. A. Dar and G. Shaviv, Technion Preprint, Technion-Ph-94-5 (1994).
7. A. M. Mukhamedzhanov and N. K. Timofeyuk, *Pisma Zh. Eksp. Teor. Fiz.* **51**, 247 (1990).
8. R. B. Kavanagh *et al.*, *Bull. Am. Phys. Soc.* **14**, 1209 (1969).
9. B. W. Filippone *et al.*, *Phys. Rev. Lett.* **50**, 412 (1983); *Phys. Rev. C* **28**, 2222 (1983).
10. C. W. Johnson *et al.*, *Astrophys. J.* **392**, 320 (1992).
11. T. Motobayashi *et al.*, RIKEN Preprint RIKKYO RUP-92-2 (1994).
12. J. N. Bahcall, *Phys. Rev.* **128**, 1297 (1962).
13. V. Castellani *et al.*, *Astron. Astrophys.* **271**, 601 (1993).
14. W. A. Fowler, *Nature* **238**, 24 (1972).
15. V. Castellani *et al.*, Istituto Nazionale Fизика Nucleare (INFN)-Ferrara Preprint INFNF-3-94 (1994).
16. K. Hirata *et al.*, *Phys. Rev. Lett.* **65**, 1301 (1990); *Phys. Rev. D* **44**, 2241 (1991).
17. B. Pontecorvo, *Atomic Energy of Canada Limited Chalk River Lab. Rep. PD-205* (1946).
18. L. W. Alvarez, *Univ. Calif. Radiat. Lab. Rep. UCRL-328* (1949).
19. P. Anselmann *et al.*, *Phys. Lett. B* **327**, 377 (1994).
20. J. N. Abdurashitov *et al.*, *Los Alamos Rep. LA-UR 94-1113* (1994); *Phys. Lett.*, in press.
21. D. R. O. Morrison, in Proceedings of the 25th International Conference on High Energy Physics, Singapore, K. K. Phua and Y. Yamaguchi, Eds. (World Scientific, Singapore 1991), p. 676.
22. S. Pakvasa, in (21), p. 698; J. N. Bahcall and H. A. Bethe, *Phys. Rev. D* **47**, 1298 (1993); M. Spiro and D. Vigneaud, *Phys. Lett. B* **242**, 279 (1990).
23. N. Hata *et al.*, *Phys. Rev. D* **49**, 3622 (1994).
24. W. Kwong and S. P. Rosen, *Phys. Rev. Lett.* **73**, 369 (1994).
25. J. N. Bahcall, Institute of Advanced Study Preprint IASSNS-AST 94/37 (1994).
26. ———, *Phys. Rev. D* **44**, 1644 (1991).
27. B. Pontecorvo, *Zh. Eksp. Teor. Fiz.* **53**, 1717 (1967); M. Nakagawa *et al.*, *Prog. Theor. Phys.* **30**, 727 (1963).
28. S. Glashow and L. Krauss, *Phys. Lett. B* **190**, 197 (1987); S. Bilenky and B. Pontecorvo, *Phys. Rep.* **41**, 225 (1978); V. Barger *et al.*, *Phys. Rev. D* **24**, 138 (1981).
29. S. P. Mikheyev and A. Smirnov, *Nuovo Cimento* **19**, 17 (1986).
30. L. Wolfenstein, *Phys. Rev. D* **20**, 2634 (1979).
31. P. Krastev and S. Petcov, *Phys. Rev. Lett.* **72**, 1960 (1994).
32. N. Hata, *Univ. Penn. Rep. UPR-0605-T* (1994).
33. ——— and P. Langacker, *Univ. Penn. Rep. UPR-0592T* (1993).
34. R. S. Raghavan, in (21), p. 482.
35. G. Bellini *et al.*, Eds., "Borexino at Gran Sasso: A Real-Time Detector for Low Energy Solar Neutrinos" (INFN-Milan Report, 1991).
36. "Borexino Progress Report" (INFN-Milan Report, 1993).
37. Y. Totsuka, *Univ. of Tokyo (ICRR) Rep. ICRR-227-90-20* (1990).
38. G. T. Ewan *et al.*, Sudbury Neutrino Observatory Proposal SNO-87-12 (1987).
39. H. Chen, *Phys. Rev. Lett.* **55**, 1534 (1985).
40. N. Hata, in (7).
41. S. Pakvasa and J. Pantaleone, *Phys. Rev. Lett.* **65**, 2479 (1990).
42. R. S. Raghavan *et al.*, *ibid.* **71**, 4295 (1993).
43. R. Lanou *et al.*, *ibid.* **58**, 2498 (1987).
44. T. Ypsilantis, in Proceedings of the II Nestor International Workshop, Univ. of Athens, Pylos, Greece, October 1993, K. Resvanis, Ed., in press.
45. E. Fiorini and T. Niinikoski, *Nucl. Instrum. Methods* **224**, 83 (1984).
46. P. F. Smith *et al.*, *Phys. Lett. B* **245**, 265 (1990).
47. I wish to thank J. Pantaleone and P. Raghavan for generous help with theoretical calculations, N. Hata for Figs. 2 and 5, and S. Pakvasa for long-standing discussions.

# High-Luminosity Blue and Blue-Green Gallium Nitride Light-Emitting Diodes

H. Morkoc and S. N. Mohammad

Compact and efficient sources of blue light for full color display applications and lighting eluded and tantalized researchers for many years. Semiconductor light sources are attractive owing to their reliability and amenability to mass manufacture. However, large band gaps are required to achieve blue color. A class of compound semiconductors formed by metal nitrides, GaN and its allied compounds AlGaN and InGaN, exhibits properties well suited for not only blue and blue-green emitters, but also for ultraviolet emitters and detectors. What thwarted engineers and scientists from fabricating useful devices from these materials in the past was the poor quality of material and lack of *p*-type doping. Both of these obstacles have recently been overcome to the point where high-luminosity blue and blue-green light-emitting diodes are now available in the marketplace.

While semiconductor coherent light sources, or lasers, continue to lure scientists and engineers, their cousins, light-emitting diodes (LEDs), have improved remarkably in terms of both brightness and the range of wavelengths of emission available (1). Early LEDs were limited to red light and luminous fluxes (2) of about 0.1 to 0.2 lm/W, which restricted their application. Over the years, red, orange, amber, and green emitters have been made with considerable enhancements in performance. With the recent introduction of blue LEDs, these emitters now span the entire range of visible wavelengths with luminous flux sufficiently high to pave the way even for outdoor LED displays and lighting.

The authors are at the University of Illinois at Urbana-Champaign, Materials Research Laboratory and Coordinated Science Laboratory, Urbana, IL 61801, USA.

Current LEDs are very reliable and have many applications. These ubiquitous devices will continue to expand their applications in displays, lighting, indicator lights, advertisement, traffic signs and traffic signals, light sources for accelerated photosynthesis, and medicine for diagnosis and treatment (3, 4). As light sources, LEDs are likely to be more efficient and reliable than incandescent lighting. In addition, white light illumination (5) by means of primary color addition is simple and has the advantage of achieving any desired color tone in the chromaticity diagram by appropriately mixing those colors in a light scrambling configuration. This requires bright green and blue sources in addition to the bright red LEDs that are already available. Made from commercially available LEDs, a display chip made in Japan uses six SiC blue, four

GaP green, two AlGaAs amber, and two AlGaAs red LEDs (6). With the recently introduced bright blue GaN-based LEDs, the number of blue devices needed can be reduced. If used in place of incandescent light bulbs, these LEDs would consume only about 10 to 20% of the power for the same luminous flux with the added advantage of compactness and much longer lifetime, 2000 hours for the former as opposed to tens of thousands for the latter.

Traffic lights at present rely on filtration of incandescent light to achieve a particular color, which is an energy-inefficient technique. Moreover, they require large repair crews for maintenance. With recently introduced blue-green 500-nm LEDs, the traffic lights can be replaced with efficient LEDs that have superior longevity. Along similar lines, the high mounted brake lights in recent model automobiles and running lights in trucks make use of red AlGaAs LEDs. It is expected that other colors will follow.

## Light Emission from Diodes

LEDs are very efficient converters of electricity to light. This phenomenon results from the intrinsic or inherent properties of the semiconductors from which they are made. Semiconductors represent an important class of materials characterized by two energy bands: the valence band and the conduction band. In an intrinsic semiconductor under normal conditions, the valence band is filled with a large number of electrons, whereas the conduction band, lying at a higher energy, is practically empty. Electrical conductivity is attributable to the transport of electrons in the conduction band and can be changed by filling the conduction band with electrons donated by appropriate impurity atoms. The electrons